Tuning Carbon-Based Fuel Cell Catalyst Support Structures via Nitrogen Functionalization. I. Investigation of Structural and Compositional Modification of Highly Oriented Pyrolytic Graphite Model Catalyst Supports as a Function of Nitrogen Implantation Dose

Svitlana Pylypenko,[†,‡] Aimee Queen,[†] Tim S. Olson,[‡] Arrelaine Dameron,[‡] Kevin O'Neill,[‡] K. C. Neyerlin,[‡] Bryan Pivovar,[‡] Huyen N. Dinh,[‡] David S. Ginley,[‡] Thomas Gennett,[‡] and Ryan O'Hayre[*,†]

[†]Department of Metallurgical & Materials Engineering, Colorado School of Mines, 1500 Illinois Street, Golden, Colorado 80401, United States

[‡]National Renewable Energy Laboratory, 1617 Cole Boulevard, Golden, Colorado 80401, United States

Ⓢ *Supporting Information*

ABSTRACT: Surface modification and doping of graphitic-carbon catalyst support materials in fuel cell systems, particularly via nitrogen functionalization, has been shown to improve catalyst performance and durability through the optimization of catalyst—support interactions. To ascertain the nature of these interactions, Raman and X-ray photoelectron spectroscopy were used to study the structural and chemical modifications that nitrogen ion beam implantation caused to highly oriented pyrolitic graphite (HOPG) model catalyst support systems. Ion implantation doses explored in this work ranged over 2 orders of magnitude from 9.0×10^{14} to 9.6×10^{16} ions cm^{-2}. Low doses of nitrogen result in a large amount of structural damage with little incorporation of nitrogen. However, it was found that with increasing dosage the incremental increase in structural damage was marginal, while the percentage of nitrogen on the HOPG surface continued to increase significantly until both the level of damage and amount of nitrogen incorporated into the graphitic structure reached saturation. A near-surface nitrogen saturation level of approximately 6—8 atomic % was achieved with a dosage equal to or greater than 2.5×10^{16} ions cm^{-2}. The nitrogen implantation altered the initial pure sp^2-hybridized graphitic carbon and resulted in the formation of sp^3-hybridized carbon while also incorporating nitrogen into the graphitic network in the graphitic, pyridinic, and pyrrolic form. This work sets the stage for understanding the effect of the amount and functionality of nitrogen on the durability of model carbon-supported fuel cell electrocatalysts, discussed in Part II (10.1021/jp112236n) of this work.
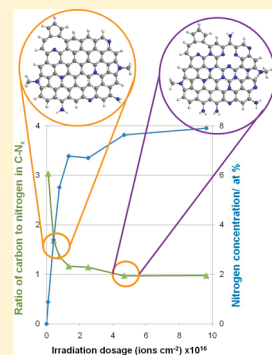
■ INTRODUCTION

Improved catalytic activity and durability are required to ensure the commercial viability of fuel cells. These issues are particularly critical in direct methanol fuel cells (DMFCs), which suffer from performance losses caused by ruthenium crossover, methanol crossover, particle growth, and incomplete oxidation of intermediate reaction products.[1−7] Recently, it was suggested that many of these losses can be mitigated through the use of functionalized supports—e.g., by surface modification or doping of the high-surface area carbon-based catalyst support materials that are commonly used in these systems.[8]

Doping with heteroatoms of nitrogen, boron, sulfur, or phosphorus has been shown to effectively modify the physical, chemical, and electronic properties of a host of carbon materials, including graphene, carbon nanotubes, and carbon black.[8−17] The primary methods of in situ doping are pyrolysis[15,18] and chemical vapor deposition.[13,19−22] In contrast, ion implantation is an ex situ doping route traditionally applied in the semiconductor industry,

although with increasing utility in a number of renewable energy applications.[9,23−27]

The performance of electrocatalysts for both the oxygen reduction reaction (ORR) and the methanol oxidation reaction (MOR) has been shown to be improved by doping the carbon support with nitrogen.[10,11,28−31] This beneficial effect has been observed on a variety of carbon supports, irrespective of the nitrogen-containing precursor or nitrogen-doping method used.[10,11,30,31] For example, Pt and Pt—Ru MOR electrocatalysts supported on nitrogen-containing carbon supports show a consistently more negative onset potential, indicative of improved intrinsic catalytic activity.[23,25,30,31] Although only a few studies report on improved intrinsic ORR catalytic activity for Pt or Pt-alloys on N-functionalized carbon supports, nearly all show evidence of improved

Table 1. Summary of Implantation Parameters and Raman and XPS Analysis Results for a Series of Nitrogen-Ion Implanted HOPG Substrates[a]

ion implantation parameters		Raman	XPS			
implantation time, s	dosage, ions cm^{-2}	I_D/I_G	carbon, at %	oxygen, at %	nitrogen, at %	C1s fwhm, eV
0	0.0×10^{16}	0.017	100	0	0	0.75
1	0.1×10^{16}	0.154	93.0	6.1	0.9	0.83
5	0.4×10^{16}	0.176	90.1	6.5	3.4	0.97
10	0.8×10^{16}	0.177	86.1	8.4	5.5	1.09
15	1.3×10^{16}	0.192	85.8	7.5	6.8	1.11
25	2.5×10^{16}	0.221	86.2	7.1	6.7	1.14
45	4.7×10^{16}	0.217	83.8	8.6	7.6	1.24
100	9.6×10^{16}	0.223	84.0	8.1	7.9	1.29

[a] Raman I_D/I_G ratios, XPS elemental composition, and C1s fwhm are listed as a function of implantation time/dosage.

nanoparticle dispersion and enhanced durability with nitrogen-functionalized supports.[12,21,32,33]

Nitrogen functional groups are specifically implicated in altering the nucleation and growth of catalyst nanoparticles (typically deposited on the carbon support using an electrochemical method), leading to improved particle size distribution and dispersion.[18,25,28] The nitrogen groups have also been suggested to enhance binding between the catalyst particles and the support[13,34−36] or to alter the electronic structure of the catalyst phase.[24,25] The detailed understanding of the exact contributions of various nitrogen functionalities, pyridinic nitrogen, in particular, toward these mechanistic aspects is not well understood. A number of studies have attempted to draw correlations between nitrogen content, typically reported to be in the range of 5−10%,[8] and the structural, chemical, and physical nature of the carbon support,[30,37] highlighting in particular the specific role of pyridinic nitrogen.[19,38]

It has been shown that compared to undoped representatives, graphitic carbon materials doped with nitrogen have a higher degree of defectiveness and edge plane sites.[39] Previously, we have compared the effects of N and Ar modification (achieved via low-energy ion implantation) on the stability and catalytic activity of electrodeposited Pt nanoparticles supported on highly oriented pyrolitic graphite (HOPG) substrates.[24,25] It was shown that physical defects, which are typically also accompanied by an increase in the oxidation sites (induced by both Ar and N implantation), and chemical modification through doping (induced only via N implantation) both result in higher site densities and smaller catalyst nanoparticle sizes. While physical defects caused by ion implantation led to improved nanoparticle distributions, only implanted nitrogen groups led to improved stability and enhanced intrinsic catalytic activity.[25]

In this work, we investigate a range of nitrogen doping levels that can be achieved using nitrogen ion implantation.[40] Since the goal is to modify only the top few nanometers of the HOPG surface, we only explore a very narrow set of implantation dosages on the lower end range of typical implantation processes, and these dosages are achieved by varying the implantation time at constant power and acceleration voltage conditions. We provide a detailed analysis of the structural and chemical modification of HOPG, used as a model graphitic carbon surface, as a function of nitrogen ion implantation conditions. Raman and X-ray photoelectron spectroscopy are used to examine the degree of defectiveness of the graphitic matrix and the appearance of specific functional groups. Understanding the specifics of support modification during nitrogen ion implantation is an important first step to elucidate the role of nitrogen concentration and functionality on the performance of fuel cell electrocatalysts.

■ EXPERIMENTAL SECTION

Substrates (10 mm × 10 mm × 1 mm) of grade 2 highly oriented pyrolytic graphite (HOPG) from SPI Inc. were employed as model carbon substrates in this work. Nitrogen ion implantation was performed at room temperature using a non-mass separated nitrogen-ion beam (N_2 and N ions) directed to the surface of the HOPG at an incident angle of 35°. Ion beam energy was kept constant at 100 eV, and ion current and time of implantation were in the range of 10−13.5 mA and 1−100 s, respectively. These conditions correlate to an estimated ion dosage in the range of 9.0×10^{14}−9.6×10^{16} ions cm^{-2}. Raman spectra were collected using a Nd:YAG laser with an excitation wavelength of 532 nm in conjunction with a double grating UHTS300 spectrometer set to the 600 g/mm option with a center wavelength of 598 nm. The setup also included a 100X Nikon objective lens and an Andor iDus CCD camera. Each single Raman spectrum resulted from 25 scans each having an integration time of 0.5 s. The D band and G band were each fitted with a Lorentzian series from which the peak intensity for each band was determined. The I_D/I_G ratio was calculated by subtracting the background from both peak intensity ratios and finally dividing the D band peak intensity by the G band peak intensity. XPS analysis was performed on a Kratos Axis Ultra X-ray photoelectron spectrometer with a monochromatic Al Kα source operated at 300 W. Survey spectra were acquired at pass energies of 80 eV with high-resolution spectra of C1s, O1s, and N1s, at 20 eV. Data analysis was performed using CasaXPS software, where a linear background subtraction was followed by charge referencing to the peak of graphitic carbon at 284.6 eV. C1s spectra of HOPG substrates doped with nitrogen were fitted using a modeling approach, where the spectrum of the undoped HOPG was used as a starting point and then additional peaks were added to complete the fit. Other spectra were treated in a traditional fashion using 70% Gaussian/30% Lorentzian line shape and constraining the full-width at half-maximum (fwhm) to 1.0 eV for C1s and N1s and to 1.3 eV for O1s. Relative amounts and standard deviations are reported for each sample as averaged from at least three areas per sample.
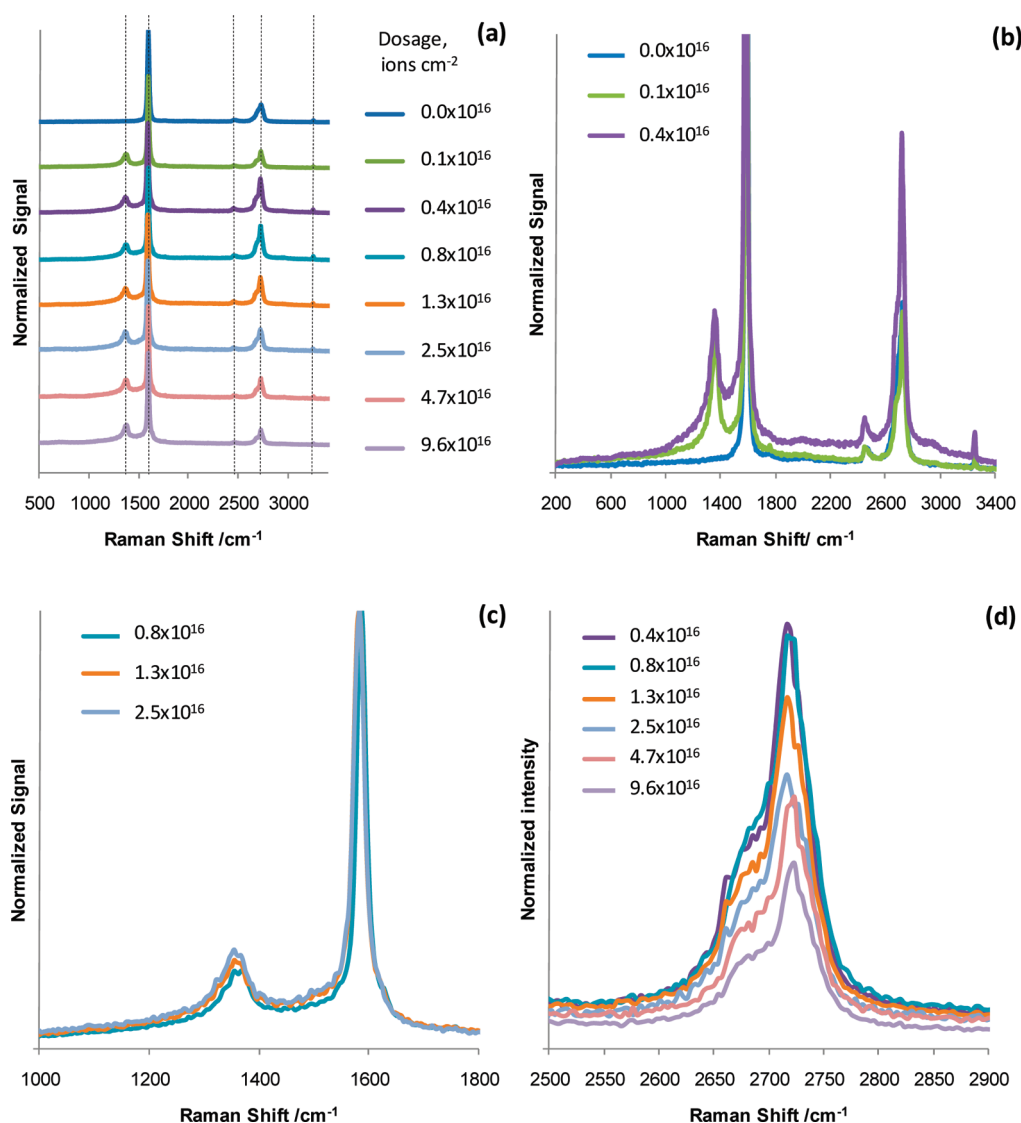
Figure 1. Representative normalized and baseline-corrected Raman spectra acquired from a series of HOPG substrates demonstrating (a) progressive changes as a function of implantation dosage, (b) effect of low implantation doses, (c) effect of medium implantation doses, and (d) effect of a range of implantation doses on the band at ~2700 cm^{-1}.

■ RESULTS AND DISCUSSION

Structural and Compositional Characterization of HOPG Substrates. Through implantation of an HOPG substrate with nitrogen, significant structural and chemical changes are observed. Raman and XPS were used to monitor these structural and chemical changes as a function of implantation time (often reported as implantation dosage). Implantation dose was estimated from the product of the implantation time and beam current density. Although the ion beam current was typically maintained in a narrow range between 10 and 13.5 mA, slight variations between implantation runs resulted in slight deviations from linearity when implantation time was converted to ion dosage. Implantation parameters (time and dosage) are listed in Table 1.

Raman. Figure 1a compares the Raman spectrum for undoped HOPG against a series of N-doped HOPG spectra. The two strong bands observed at ~1590 and 2700 cm^{-1} are the G band (tangential mode) and G′ band (interlayer coupling), respectively.
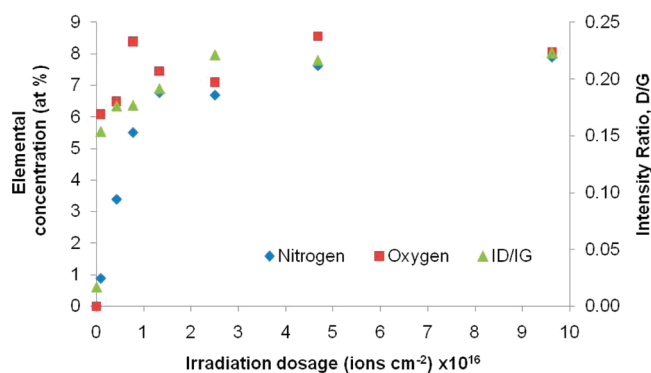
Figure 2. Correlation between nitrogen and oxygen concentrations and ratio of intensities of Raman D band and G band (I_D/I_G), shown as a function of implantation dosage.

The G′ band at ~2700 cm^{-1} along with the small band at ~3250 cm^{-1} are indicative of well-ordered crystalline graphitic
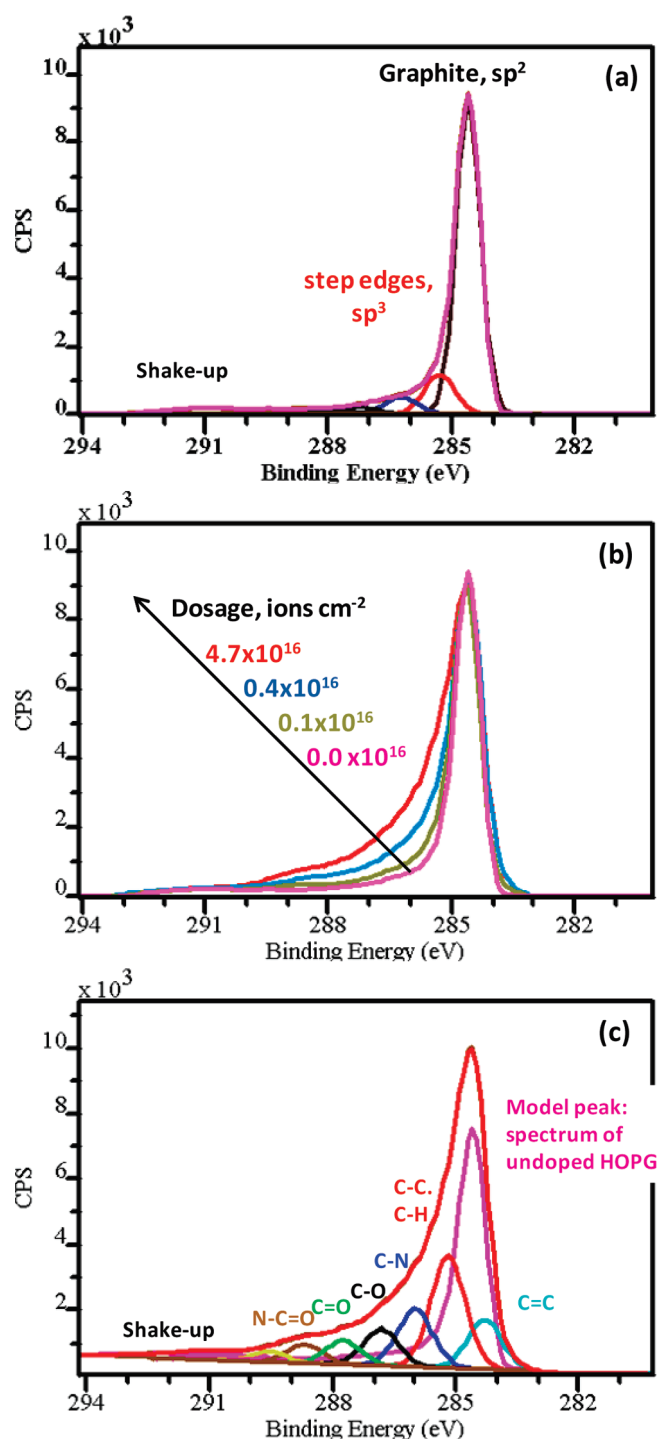
Figure 3. High-resolution XPS C 1s spectra of (a) undoped HOPG, curve-fitted, (b) overlay of normalized undoped HOPG and HOPG implanted with the following nitrogen ion dosages: 0.1×10^{16}, 0.4×10^{16}, and 4.7×10^{16} ions cm^{-2}, and (c) HOPG implanted with 4.7×10^{16} ions cm^{-2}, curve-fitted.

carbon. Another small band, characteristic of the basal plane of graphite, is also observed in the spectrum of undoped HOPG at ~2450 cm^{-1}.

Compared to undoped HOPG, all N-doped HOPGs show a significant increase in structural disorder, evident from the appearance of the D band at ~1350 cm^{-1}. Figure 1b demonstrates that

even the lowest implantation dose (0.1×10^{16} ions cm^{-2}, 1 s) used in this study resulted in the appearance of a well-resolved D band, indicating that even extremely short implantation times are sufficient to induce significant structural changes of the HOPG surface. The ratio of the D vs G band intensities (I_D/I_G) is widely used as a measure of the disorder of carbon-based materials.[19,25] In Figure 2, the I_D/I_G ratios for all analyzed samples are displayed as a function of implantation dose. An increase in the I_D/I_G ratio from 0.017 for the undoped HOPG to 0.154 (after 0.1×10^{16} ions cm^{-2}, 1 s N-implantation) and 0.176 (after 0.4×10^{16} ions cm^{-2}, 5 s N-implantation) is also accompanied by a significant broadening of the D band. While 0.1×10^{16} ions cm^{-2} (1 s) N-implantation results in little or no change to the bands above 2200 cm^{-1}, significant changes to these bands are observed after 0.4×10^{16} ions cm^{-2} (5 s) N-implantation, and in particular, a new wide band appears at ~2955 cm^{-1} which is characteristic of edge-plane carbon (Figure 1b). A possible explanation for this observation is that at the initial stages of implantation surface damage is accompanied by surface "cleaning". The Raman spectra for implantation dosages greater than 0.4×10^{16} ions cm^{-2} (5 s) reveal only incremental changes (Figure 1c), with gradual broadening and intensity increase of the D band (and thus I_D/I_G). No further changes are observed for implantation doses $\geq2.5 \times 10^{16}$ ions cm^{-2} (25 s) (Figure 2). Meanwhile, the intensity of the bands at ~2700 and ~3250 cm^{-1} continually decreases with implantation dose (Figure 1d). Thus, although the overall degree of HOPG structural damage reaches saturation after a dose of 2.5×10^{16} (~25 s), the near-surface layers continue to undergo minor changes with further increase in implantation dose (as reflected by the decreased intensity of the interlayer coupling and ordering bands at ~2700 and ~3250 cm^{-1}). The observation of apparent saturation in the Raman results is perhaps not too surprising, considering the highly surface-sensitive nature of both the ion implantation and Raman characterization. On the basis of previous estimates from SRIM modeling,[25] low-energy (100 eV) ion implantation of nitrogen into graphite affects only the near-surface region (certainly less than 5−10 nm deep), similar to (if not already greater than) the depth sensitivity of Raman measurement. Accounting for these implantation depths, implantation dosages of $>2.5 \times 10^{16}$ ions cm^{-2} translate into volumetric implantation levels of ~1 ion/carbon atom or higher, a level which is clearly consistent with a saturation of surface damage effects.

XPS. Undoped and N-doped HOPG were also characterized by XPS analysis to evaluate both elemental and chemical surface composition. In freshly cleaved undoped HOPG, carbon is the only element detected by XPS—neither nitrogen nor oxygen is found. A typical high-resolution C1s spectrum of undoped HOPG is presented in Figure 3a. As is typical for graphitic carbon, the C1s spectrum of undoped HOPG is a very narrow peak with asymmetrical broadening on the high binding energy side.[41−43] Details of the fitting approach used for the C1s peak of undoped HOPG are provided in the Supporting Information.

XPS analysis of the N-doped HOPG samples as a function of N implantation dose reveals significant chemical and structural changes. Consistent with the Raman measurements, the XPS studies reveal rapid changes at low implantation dosages before saturation is observed after dosages of $\sim1.3−2.5 \times 10^{16}$ ions cm^{-2} ($\sim15−25$ s). Table 1 and Figure 2 summarize the trends observed for elemental composition of the HOPG surface as a function of the implantation dose. Chemical incorporation of nitrogen is evident from the gradual increase in the nitrogen
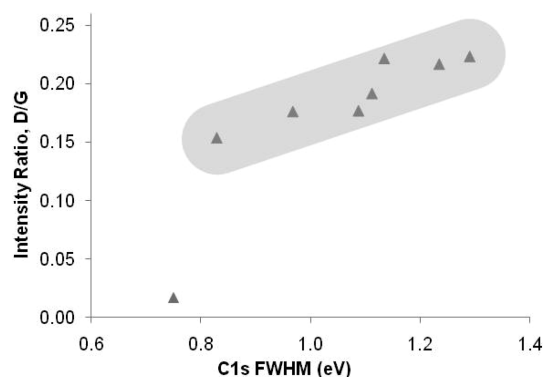
Figure 4. Correlations between fwhm of the XPS high-resolution C1s spectrum and ratio of intensities of the Raman D band to G band (I_D/I_G).

concentration during the first 1.3×10^{16} ions cm^{-2} (15 s) of implantation, before a plateau is observed at ~6−8 at %, suggesting that graphitic carbon reaches the point of saturation with nitrogen doping at these concentration levels. Structural modification of the HOPG, however, is not limited to implantation of chemically bound nitrogen. In fact, oxygen surface species increase more rapidly than nitrogen species during the initial N-implantation stages (0.1×10^{16}−0.4×10^{16} ions cm^{-2}, 1−5 s). While no oxygen species were detected on undoped HOPG, after just 0.1×10^{16} ions cm^{-2} (1 s) of N-implantation the oxygen concentration of the HOPG surface reaches 6 at %. The surface oxygen content continues to increase to about 8 at % after 0.8×10^{16} ions cm^{-2} (10 s) implantation before reaching a plateau. This behavior suggests that reactive surface defects (i.e., dangling bonds, step edges, radicals, etc.) created by the implantation process are immediately passivated and/or oxidized by oxygen species upon exposure to atmosphere.

Figure 2 illustrates both the physical and chemical modification trends during nitrogen implantation. The I_D/I_G ratio calculated from the Raman data provides a rough measure of the total defect damage introduced by implantation, while the elemental oxygen and nitrogen composition trends obtained from XPS highlight only the chemical modification processes. As a comparison of these data sets reveals, the first 0.09×10^{16}−0.4×10^{16} ions cm^{-2} (1−5 s) of irradiation results in significant physical damage to the HOPG (and subsequently a significant degree of oxygen surface modification) but very little nitrogen incorporation. However, with continued implantation up to ~1.0×10^{16} ions cm^{-2}, the nitrogen incorporation increases significantly although little additional physical damage is observed. Further increase in the ion dose from 1.3×10^{16}−2.50×10^{16} up to 9.6×10^{16} ions cm^{-2} did not appear to affect either the I_D/I_G ratio or elemental composition but did continue to affect the surface order of the HOPG as revealed by continued evolution of the higher-order Raman bands.

Further details of the structural modification during implantation can be attained through analysis of high-resolution XPS spectra. As shown in Figure 3b and 3c, N-implantation eliminates the broad shake-up peak positioned at about 291 eV. The disappearance of this shake-up peak indicates a loss of delocalization in the carbon structure of the N-implanted HOPG. At the same time, loss of the shake-up peak is accompanied by obvious C1s peak broadening. Figure 3a and Figure 4 illustrate that the fwhm increases with increasing N implantation dosage and

clearly shows the correlation between the Raman and XPS data. Similar fwhm broadening trends have been observed for high surface area N-doped carbons.[19] The broadening of the C1s spectra is highly asymmetric, leading, with increasing implantation doses, to the development of a distinct shoulder at high binding energies (~285−290 eV) (Figure 3b). The nature of the carbon defects and chemical dopants associated with this high-binding energy peak broadening can be obtained from further analysis of C1s spectra through the application of curve-fitting as detailed in the following paragraphs.

To quantify relatively minor changes in the C1s spectra of a series of modified HOPG substrates, we adopt a modeling-based curve-fitting approach using the undoped HOPG as a reference standard.[44,45] As shown in Table 2, as the implantation dose increases, the HOPG becomes increasingly modified as reflected by a diminishing contribution from the "unmodified" standard in the overall spectrum fit. The degree of modification increases rapidly to ~50% after only 0.8×10^{16} ions cm^{-2} (10 s) of implantation. At higher implantation dosages the rate of modification slows down considerably. This result is consistent with saturation of nitrogen and oxygen as well as Raman I_D/I_G ratios at higher implantation doses.

Among various new peaks in the C1s spectra of modified HOPG, perhaps most important are the appearance of peaks associated with sp^2 and sp^3 hybridized carbon as well as peaks associated with carbon−nitrogen bonding and carbon−oxygen bonding. With increasing implantation time, both sp^2- and sp^3-hybridized carbon increase, although the sp^3 carbon increases more rapidly. The peak at 286.1 eV is due to the formation of C−N bonding;[46] the ratio of carbon atoms bonded to nitrogen versus the total concentration of nitrogen can be used to estimate number of carbon atoms per nitrogen atom. Figure 5a displays estimated values of this ratio as a function of implantation dose. As this figure shows, single substitutional nitrogen defects bonded to three carbon atoms are only likely at the lowest implantation dose of 0.1×10^{16} ions cm^{-2} (1 s). At higher implantation doses, the bonding ratio rapidly decreases to ~1.5 and even 1. Such a dramatic change in the ratio indicates the formation of defect-complex functionalities where carbon atoms are bonded to more than one nitrogen atom. This suggests that as the implantation dose increases the N dopants preferentially cluster into groups rather than remain as isolated N substitutional defects. This finding is also substantiated by DFT modeling calculations, which suggest that the formation of multinitrogen defect clusters is energetically preferred versus the formation of single isolated nitrogen defects.[47]

The fitting peaks at 286.9, 287.8, and 288.8 eV (Figure 3c and Table 2) are attributed mostly to C−O, C=O, and O−C=O, although the latter two peaks could also contain contributions from N−C−O and N−C=O, respectively.[46] Detailed analysis of O1s was consistent with C1s and N1s but did not provide additional insight. Figure 5b compares the amount of oxygen associated with these three C1s peaks versus the total amount of oxygen detected from the O1s spectra for each sample. At the lowest implantation dose, 0.1×10^{16} ions cm^{-2} (1 s), the total concentration of oxygen detected on the HOPG (~6 at %) is approximately twice as large as the concentration of oxygen that can be attributed to the carbon−oxygen bond peaks. This implies that about half of the oxygen species observed in this sample is bonded while the other half is chemically adsorbed to the surface of HOPG. At higher implantation doses, however, the C1s bonded oxygen concentration increases significantly (to as high

Table 2. Quantification of High-Resolution C1s XPS Spectra for a Series of N Implanted HOPG Substrates[a]

ID	model-HOPG	sp^2	sp^3	C−N	C−O	C=O, N−C−O	O−C=O, N−C=O	shakeup	ratio, sp^3/sp^2
BE, eV	284.6	284.3	285.2	286.1	286.9	287.8	288.8	290−292	
Dosage, ions cm^{-2}						Relative Amount, %			
0.0×10^{16}	100.0	0.0	0.0	0.0	0.0	0.0	0.0	0	
0.1×10^{16}	78.6	7.6	7.2	2.9	0.0	1.6	1.6	0.5	0.9
0.4×10^{16}	61.4	9.1	12.4	6.3	3.9	3.6	2.1	1.1	1.4
0.8×10^{16}	50.4	10.2	15.7	8.7	5.4	3.3	3.1	3.2	1.5
1.3×10^{16}	47.0	11.3	16.0	9.2	5.8	4.1	3.2	3.5	1.4
2.5×10^{16}	46.9	11.2	16.4	9.1	5.9	4.3	3.3	2.9	1.5
4.7×10^{16}	42.7	12.0	20.3	8.9	5.9	3.2	4.0	3.2	1.7
9.6×10^{16}	44.1	11.3	19.8	9.2	6.1	4.0	3.0	2.6	1.7

[a] The spectrum of the undoped HOPG was used as a model peak during curve-fitting of the spectra for the doped HOPG samples.
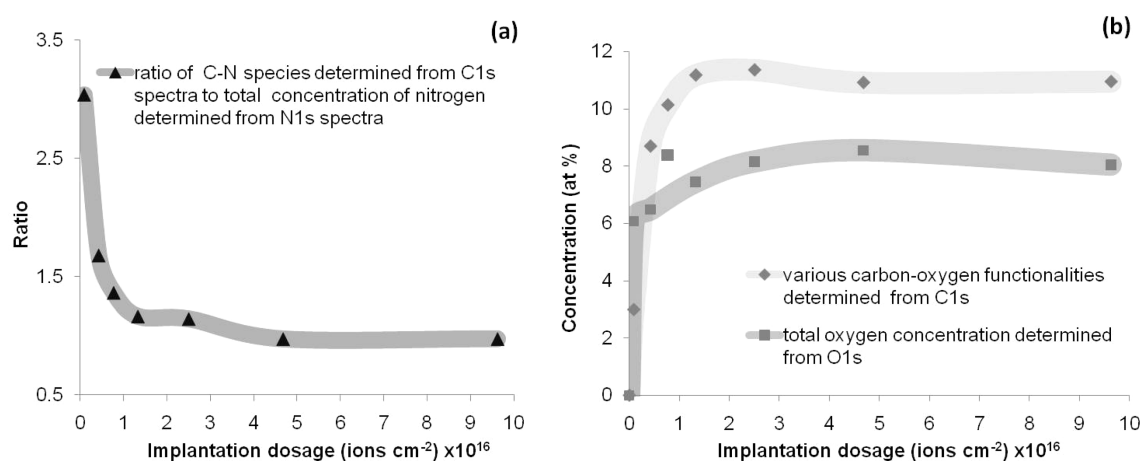

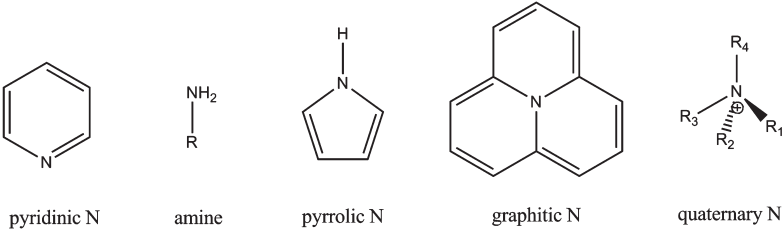**Figure 5.** Major trends observed for nitrogen and oxygen functionalities.

as 12 at %), while the total oxygen concentration as determined from the O1s peak increases only marginally (to ∼8 at %). Even though combined oxygen—carbon—nitrogen groups are likely to contribute more appreciably to the intensity of these carbon—oxygen peaks at higher implantation levels, our estimation of carbon—oxygen species present in the HOPG is still inflated. This discrepancy could be a result of the limitation of our C1s peak modeling approach that assumes that part of HOPG stays unchanged. It is likely that the band structure of HOPG, and therefore its asymmetric line-shape, are affected by the implantation. Shake-up peaks from the lower BE components are likely superimposed on these carbon—oxygen peaks, making quantification difficult. Sacher et al. have attributed a peak at 287.8 eV to the shakeup of the localized aromatic bonds formed during Ar$^+$ modification of HOPG.[48] Importantly, aromatic nitrogen-containing compounds are also known to give rise to shake-up features that lie in this binding energy range.

A representative high-resolution N1s spectrum obtained from HOPG after ion implantation is shown in Figure 6, demonstrating that the spectrum is fairly wide and indicating the presence of a variety of nitrogen functionalities.[17,19,21,49−53] Though the binding energy range is typical of nitrogen-doped carbon materials, there are some differences in the shape of the spectrum that are important to note. For example, N1s spectra typically
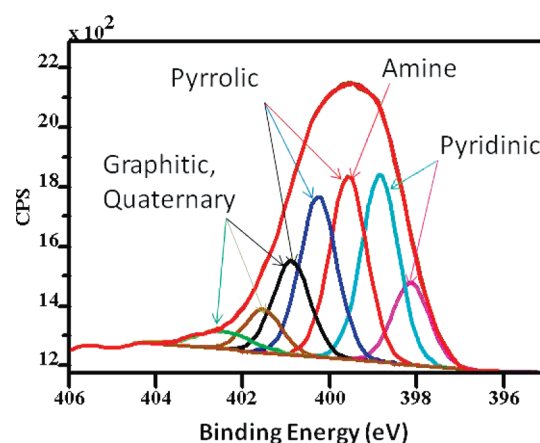
Figure 6. High-resolution N1s XPS spectra of HOPG implanted with 4.7×10^{16} ions cm^{-2}.

reported for nitrogen-doped CNTs and carbon blacks, prepared using nitrogen-containing precursors, have two or three distinctive peaks.[19,39] The peak at low BE is due to pyridinic N, and the peak at higher BE, typically fitted with one or two peaks, is due to quaternary/graphitic and/or pyrrolic N. The N1s spectra from

13672

dx.doi.org/10.1021/jp1122344 |J. Phys. Chem. C 2011, 115, 13667–13675

Table 3. Quantification of High-Resolution N1s XPS Spectra for a Series of N Implanted HOPG Substrates[a]

ID	Pyridinic		Amine, Pyrrolic	Pyrrolic	Pyrrolic, Graphitic, Quaternary	Graphitic, Quaternary	Graphitic, Quaternary
BE, eV	398.1	398.8	399.5	400.1	400.9	401.8	402.9
Dosage, ions cm^{-2}	Relative amount, %						
0.1x10^{16}	2.7 (4.6)	7.0 (6.1)	23.2 (3.1)	32.0 (4.4)	25.4 (4.6)	7.7 (3.6)	2.1 (3.6)
0.4x10^{16}	11.4 (1.2)	22.5 (0.6)	22.4 (1.4)	21.2 (1.5)	12.4 (1.3)	5.3 (1.6)	4.8 (0.8)
0.8x10^{16}	12.8 (0.7)	22.7 (0.6)	24.2 (0.6)	21.5 (1.2)	10.9 (1.4)	4.6 (1.5)	3.3 (0.4)
1.3x10^{16}	11.9 (1.0)	24.7 (1.0)	22.3 (1.1)	20.7 (0.5)	12.1 (0.6)	4.4 (0.2)	3.9 (0.7)
2.5x10^{16}	11.7 (1.2)	24.7 (1.9)	22.4 (0.4)	19.4 (0.4)	12.4 (0.1)	6.6 (0.5)	2.9 (0.7)
4.7x10^{16}	10.4 (0.4)	24.4 (0.4)	23.4 (0.2)	20.5 (0.9)	12.5 (0.5)	5.2 (0.9)	3.6 (0.7)
9.6x10^{16}	10.9 (0.6)	23.7 (2.2)	23.3 (0.6)	21.2 (1.7)	11.9 (1.6)	5.0 (1.3)	4.1 (0.8)
0.4x10^{16}-9.6x10^{16}	11.5 (0.8)	23.8 (1.0)	23.0 (0.8)	20.7 (0.8)	12.0 (0.6)	5.2 (0.8)	3.8 (0.7)

pyridinic N   amine   pyrrolic N   graphitic N   quaternary N

[a] Relative amounts and standard deviations (in brackets) are reported for each sample as an average from at least three areas. The last row reports average and standard deviation (in brackets) for the range of the implantation dosages.

N-doped HOPG, on the other hand, are wide but without distinctive peaks. To provide consistent comparison between samples after various dosages, peak fitting was therefore performed using constraints on the peak widths and positions. Peak positions and nitrogen functionalities that can potentially contribute to these peaks are listed in Table 3. From a series of HOPG samples, only the sample with the lowest doping level, 0.1×10^{16} ions cm^{-2} (1 s), showed a significantly different distribution of nitrogen functionalities. It also had higher standard deviation, which we attribute to the low overall concentration and inhomogeneity of implanted nitrogen in this sample due to the short implantation time (resulting in a high signal-to-noise ratio). The majority of the nitrogen in this sample is found in graphitic, pyrrolic, and possibly amine forms with only small amounts of pyridinic types. An increase in the dosage up to 0.4×10^{16} ions cm^{-2} results in a significant increase in pyridinic-type nitrogen. All higher implantation dosages (e.g., from 0.4×10^{16} to 9.6×10^{16} ions cm^{-2}) result in similar distributions of nitrogen functionalities and fairly similar standard deviations calculated based on the analysis of at least three different areas for each sample. The averages and standard deviations among the samples with implantation dosages 0.4×10^{16}–9.6×10^{16}

ions cm^{-2} are only marginally different from the ones that are calculated for each dosage separately. Earlier, in the discussion of the Figure 5a, we concluded that the increase in the nitrogen concentration at higher implantation times results in the formation of clusters of multinitrogen defects. In conclusion, an increase in the implantation dosage affects the amount of implanted nitrogen and increases the concentration of clusters of defects with more than one nitrogen substitution.

■ SUMMARY

XPS and Raman are used to evaluate the structural disorder of HOPG as a function of nitrogen implantation. As the ion implantation dose increases from 0.1×10^{16} ions cm^{-2} (1 s) to 2.5×10^{16} ions cm^{-2} (25 s), the degree of structural disorder and the amount of implanted nitrogen also increase. Low implantation doses result in significant physical damage with incorporation of small amounts of nitrogen; higher implantation dosages are required to achieve significant nitrogen incorporation. Oxygen functionalization accompanies the nitrogen ion implantation process, likely due to passivation of physical defects by oxygen during ambient air exposure of the graphite surfaces.

13673

dx.doi.org/10.1021/jp1122344 |J. Phys. Chem. C 2011, 115, 13667–13675

Saturation levels for both physical damage and nitrogen loading are achieved after about 25 s of implantation (corresponding to implantation doses of ∼2.5 × 10^{16} ions cm^{-2} or greater). Both oxygen and nitrogen species appear to reach surface saturation at ∼6−8 at % concentration levels. Mostly pure sp^2-hybridized carbon in unmodified HOPG is altered during implantation, with the formation of sp^3-hybridized carbon as well as the appearance of carbon−nitrogen and carbon−oxygen bonding. Various types of nitrogen functionalities are detected on the surface of modified HOPG, indicating that implantation results in the incorporation of nitrogen into the graphitic network via the formation of graphitic-type nitrogen as well as increases in the edge-plane sites through the formation of pyridinic and pyrrolic types of nitrogen. Implantation dosages in the range of 0.4 × 10^{16}−9.6 × 10^{16} ions cm^{-2} result in a similar distribution of nitrogen functionalities. The major distinction between high implantation doses and low-to-medium implantation doses is the amount of doped nitrogen and, interestingly, the presence of the clustered multinitrogen defects. The specific role of nitrogen functionalities and, in particular these clustered defects, on the stability of Pt−Ru catalyst nanoparticles is further discussed in Part II (10.1021/jp112236n) of this work.

ASSOCIATED CONTENT

S **Supporting Information.** Details of the fitting approach used for the C1s peak of undoped HOPG and discussion of modeling approach used to curve-fit C1s of modified HOPG. This material is available free of charge via the Internet at http://pubs.acs.org.

AUTHOR INFORMATION

Corresponding Author
*E-mail: rohayre@mines.edu.

ACKNOWLEDGMENT

REFERENCES

(1) Arico, A. S.; Creti, P.; Poltarzewski, Z.; Mantegna, R.; Kim, H.; Giordano, N.; Antonucci, V. *Mater. Chem. Phys.* **1997**, *47*, 257.

(2) Borup, R.; Meyers, J.; Pivovar, B.; Kim, Y. S.; Mukundan, R.; Garland, N.; Myers, D.; Wilson, M.; Garzon, F.; Wood, D.; Zelenay, P.; More, K.; Stroh, K.; Zawodzinski, T.; Boncella, J.; McGrath, J. E.; Inaba, M.; Miyatake, K.; Hori, M.; Ota, K.; Ogumi, Z.; Miyata, S.; Nishikata, A.; Siroma, Z.; Uchimoto, Y.; Yasuda, K.; Kimijima, K. I.; Iwashita, N. *Chem. Rev.* **2007**, *107*, 3904.

(3) Cheng, T. T. H.; Jia, N. Y.; He, P. *J. Electrochem. Soc.* **2010**, *157*, B714.

(4) Eickes, C.; Piela, P.; Davey, J.; Zelenay, P. *J. Electrochem. Soc.* **2006**, *153*, A171.

(5) Park, G. S.; Pak, C.; Chung, Y. S.; Kim, J. R.; Jeon, W. S.; Lee, Y. H.; Kim, K.; Chang, H.; Seung, D. *J. Power Sources* **2008**, *176*, 484.

(6) Piela, P.; Eickes, C.; Brosha, E.; Garzon, F.; Zelenay, P. *J. Electrochem. Soc.* **2004**, *151*, A2053.

(7) Shyam, B.; Arruda, T. M.; Mukerjee, S.; Ramaker, D. E. *J. Phys. Chem. C* **2009**, *113*, 19713.

(8) Zhou, Y. K.; Neyerlin, K.; Olson, T. S.; Pylypenko, S.; Bult, J.; Dinh, H. N.; Gennett, T.; Shao, Z. P.; O'Hayre, R. *Energy Environ. Sci.* **2010**, *3*, 1437.

(9) Bangert, U.; Bleloch, A.; Gass, M. H.; Seepujak, A.; van den Berg, J. *Phys. Rev. B* **2010**, *81*.

(10) Lei, Z. B.; An, L. Z.; Dang, L. Q.; Zhao, M. Y.; Shi, J. Y.; Bai, S. Y.; Cao, Y. D. *Microporous Mesoporous Mater.* **2009**, *119*, 30.

(11) Lei, Z. B.; Zhao, M. Y.; Dang, L. Q.; An, L. Z.; Lu, M.; Lo, A. Y.; Yu, N. Y.; Liu, S. B. *J. Mater. Chem.* **2009**, *19*, 5985.

(12) Li, X. G.; Park, S.; Popov, B. N. *J. Power Sources* **2010**, *195*, 445.

(13) Maldonado, S.; Stevenson, K. J. *J. Phys. Chem. B* **2005**, *109*, 4707.

(14) Ozaki, J.; Anahara, T.; Kimura, N.; Oya, A. *Carbon* **2006**, *44*, 3358.

(15) Pocard, N. L.; Alsmeyer, D. C.; Mccreery, R. L.; Neenan, T. X.; Callstrom, M. R. *J. Mater. Chem.* **1992**, *2*, 771.

(16) Prehn, K.; Warburg, A.; Schilling, T.; Bron, M.; Schulte, K. *Compos. Sci. Technol.* **2009**, *69*, 1570.

(17) Terrones, M.; Redlich, P.; Grobert, N.; Trasobares, S.; Hsu, W. K.; Terrones, H.; Zhu, Y. Q.; Hare, J. P.; Reeves, C. L.; Cheetham, A. K.; Ruhle, M.; Kroto, H. W.; Walton, D. R. M. *Adv. Mater.* **1999**, *11*, 655.

(18) Ye, S. Y.; Vijh, A. K.; Dao, L. H. *J. Electrochem. Soc.* **1996**, *143*, L7.

(19) Maldonado, S.; Morin, S.; Stevenson, K. J. *Carbon* **2006**, *44*, 1429.

(20) Vijayaraghavan, G.; Stevenson, K. J. *Langmuir* **2007**, *23*, 5279.

(21) Sun, C. L.; Chen, L. C.; Su, M. C.; Hong, L. S.; Chyan, O.; Hsu, C. Y.; Chen, K. H.; Chang, T. F.; Chang, L. *Chem. Mater.* **2005**, *17*, 3749.

(22) Chen, L. C.; Wen, C. Y.; Liang, C. H.; Hong, W. K.; Chen, K. J.; Cheng, H. C.; Shen, C. S.; Wu, C. T.; Chen, K. H. *Adv. Funct. Mater.* **2002**, *12*, 687.

(23) Chetty, R.; Kundu, S.; Xia, W.; Bron, M.; Schuhmann, W.; Chirila, V.; Brandl, W.; Reinecke, T.; Muhler, M. *Electrochim. Acta* **2009**, *54*, 4208.

(24) Zhou, Y. K.; Holme, T.; Berry, J.; Ohno, T. R.; Ginley, D.; O'Hayre, R. *J. Phys. Chem. C* **2010**, *114*, 506.

(25) Zhou, Y. K.; Pasquarelli, R.; Holme, T.; Berry, J.; Ginley, D.; O'Hayre, R. *J. Mater. Chem.* **2009**, *19*, 7830.

(26) Grigull, S.; Jacob, W.; Henke, D.; Spaeth, C.; Summchen, L.; Sigle, W. *J. Appl. Phys.* **1998**, *83*, 5185.

(27) Gouzman, I.; Brener, R.; Hoffman, A. *J. Vac. Sci. Technol. A* **1999**, *17*, 411.

(28) Roy, S. C.; Christensen, P. A.; Hamnett, A.; Thomas, K. M.; Trapp, V. *J. Electrochem. Soc.* **1996**, *143*, 3073.

(29) Shukla, A. K.; Ravikumar, M. K.; Roy, A.; Barman, S. R.; Sarma, D. D.; Arico, A. S.; Antonucci, V.; Pino, L.; Giordano, N. *J. Electrochem. Soc.* **1994**, *141*, 1517.

(30) Maiyalagan, T. *Appl. Catal., B* **2008**, *80*, 286.

(31) Wu, G.; Li, D. Y.; Dai, C. S.; Wang, D. L.; Li, N. *Langmuir* **2008**, *24*, 3566.

(32) Groves, M. N.; Chan, A. S. W.; Malardier-Jugroot, C.; Jugroot, M. *Chem. Phys. Lett.* **2009**, *481*, 214.

(33) Roy, S. C.; Harding, A. W.; Russell, A. E.; Thomas, K. M. *J. Electrochem. Soc.* **1997**, *144*, 2323.

(34) Ye, S. Y.; Vijh, A. K.; Dao, L. H. *J. Electrochem. Soc.* **1997**, *144*, 90.

(35) Maiyalagan, T.; Viswanathan, B.; Varadaraju, U. *Electrochem. Commun.* **2005**, *7*, 905.

(36) Chen, Y. G.; Wang, J. J.; Liu, H.; Li, R. Y.; Sun, X. L.; Ye, S. Y.; Knights, S. *Electrochem. Commun.* **2009**, *11*, 2071.

(37) Wiggins-Camacho, J. D.; Stevenson, K. J. *J. Phys. Chem. C* **2009**, *113*, 19082.

(38) Kurak, K. A.; Anderson, A. B. *J. Phys. Chem. C* **2009**, *113*, 6730.

(39) Matter, P. H.; Zhang, L.; Ozkan, U. S. *J. Catal.* **2006**, *239*, 83.

(40) Pylypenko, S.; Queen, A.; Neyerlin, K. C.; Olson, T.; Dameron, A.; O'Neill, K.; Ginley, D.; Gorman, B.; Kocha, S.; Dinh, H. N.; Gennett, T.; O'Hayre, R. *ECS Trans.* **2010**, *33*, 351.

(41) Estrade-Szwarckopf, H. *Carbon* **2004**, *42*, 1713.

(42) Yang, D. Q.; Sacher, E. *Langmuir* **2006**, *22*, 860.

(43) Larachi, F.; Dehkissia, S.; Adnot, A.; Chornet, E. *Energy Fuels* **2004**, *18*, 1744.

13674

dx.doi.org/10.1021/jp1122344 |*J. Phys. Chem. C* 2011, 115, 13667–13675

(44) Artyushkova, K.; Levendosky, S.; Atanassov, P.; Fulghum, J. *Top. Catal.* **2007**, *46*, 263.

(45) Artyushkova, K.; Fulghum, J. E. *Surf. Interface Anal.* **2001**, *31*, 352.

(46) Beamson, G. B., D. *High Resolution XPS of Organic Polymers: The Scienta ESCA300 Database*; Wiley, Chichester: New York, 1992.

(47) Holme, T.; Zhou, Y. K.; Pasquarelli, R.; O'Hayre, R. *Phys. Chem. Chem. Phys.* **2010**, *12*, 9461.

(48) Yang, D. Q.; Sacher, E. *Surf. Sci.* **2002**, *516*, 43.

(49) Kusunoki, I.; Sakai, M.; Igari, Y.; Ishidzuka, S.; Takami, T.; Takaoka, T.; Nishitani-Gamo, M.; Ando, T. *Surf. Sci.* **2001**, *492*, 315.

(50) Artyushkova, K.; Pylypenko, S.; Olson, T. S.; Fulghum, J. E.; Atanassov, P. *Langmuir* **2008**, *24*, 9082.

(51) Jaouen, F.; Herranz, J.; Lefevre, M.; Dodelet, J. P.; Kramm, U. I.; Herrmann, I.; Bogdanoff, P.; Maruyama, J.; Nagaoka, T.; Garsuch, A.; Dahn, J. R.; Olson, T.; Pylypenko, S.; Atanassov, P.; Ustinov, E. A. *ACS Appl. Mater. Interfaces* **2009**, *1*, 1623.

(52) Pylypenko, S.; Mukherjee, S.; Olson, T. S.; Atanassov, P. *Electrochim. Acta* **2008**, *53*, 7875.

(53) Olson, T. S.; Pylypenko, S.; Atanassov, P.; Asazawa, K.; Yamada, K.; Tanaka, H. *J. Phys. Chem. C* **2010**, *114*, 5049.